Orbital-selective superconductivity, gap anisotropy, and spin resonance excitations in a multiorbital t-J_1-J_2 model for iron pnictides

Rong Yu,[1,2] Jian-Xin Zhu,[3] and Qimiao Si[2]

[1]*Department of Physics, Renmin University of China, Beijing 100872, China*

[2]*Department of Physics & Astronomy, Rice University, Houston, Texas 77005, USA*

[3]*Theoretical Division and Center for Integrated Nanotechnologies, Los Alamos National Laboratory, Los Alamos, New Mexico 87545, USA*

(Received 20 June 2013; revised manuscript received 22 December 2013; published 22 January 2014)

We study the orbital-selective superconducting pairing in a five-orbital t-J_1-J_2 model for iron pnictides. Depending on the orbital selectivity of electron correlations and the orbital characters along the Fermi surface, the superconducting gap in an A_{1g} pairing state may exhibit anisotropy. This anisotropy varies with the degree of J_1-J_2 magnetic frustration. In the superconducting state, the frequency dependence of the dynamical spin susceptibility at the antiferromagnetic wave vector $(\pi,0)$ shows a resonance, whose width is enhanced by the orbital selectivity of the superconducting gap. When the degree of the orbital selectivity is sufficiently strong, the resonance peak may be split in two. We discuss the implications of our results on the recent angle-resolved photoemission and neutron-scattering measurements in several superconducting iron pnictides.

DOI: 10.1103/PhysRevB.89.024509 PACS number(s): 71.30.+h, 71.10.Hf, 71.27.+a, 74.70.Xa

I. INTRODUCTION

One of the central questions in the field of unconventional superconductivity is whether a single mechanism operates across a variety of superconducting (SC) materials, such as iron pnictides, cuprates, heavy fermions, and organic superconductors. In many cases, including for the iron-based superconductors [1–3], superconductivity arises at the border of antiferromagnetic order and electron correlations make the normal state a bad metal. As such, it is desirable to provide an affirmative answer to this question. At the same time, there are some important apparently distinct features in the different material classes. For example, for many heavy fermions, quantum criticality is clearly important, raising the question of whether it is also relevant for the other materials families. In the same vein, there is rapidly growing evidence that multiorbital physics plays an important role in the properties of the iron-based materials, raising the possibility that this physics in general, and orbital selectivity in particular, is not only important to the iron-based materials, but it also represents a mechanism that boosts the SC pairing in general.

Orbital selectivity in the normal state of the iron pnictides and chalcogenides has recently been studied extensively [4–9]. *Nondegenerate* Fe 3d orbitals, particularly the xz/yz and xy orbitals, yield different mass renormalization and, in the extreme case, an orbitally selective Mott phase. Evidence for such orbital selectivity has come from angle-resolved photoemission spectroscopy (ARPES) measurements [10,11]. To ascertain how orbital-selective correlations may contribute to superconductivity, it is imperative to address how the orbital selectivity affects the nature and properties of the SC state.

Here we ask how orbital selectivity affects spin resonance excitation, which has been studied for over 20 years in cuprates [12] and has also been studied in iron-based superconductors since the field's inception [13–16]. The specific approach we will take is motivated by two considerations. First, neutron resonance is generally considered to be a spin-triplet excitonic excitation formed out of the electronic and hole quasiparticles of an unconventional superconductor. Second, in iron pnictides, the orbital weight varies on both the hole Fermi pockets near the center of the Brillouin zone (BZ) and the electron Fermi pockets near the edge of the (one-Fe-unit-cell) BZ. The orbital-weight variation on the hole Fermi pocket is primarily among the degenerate 3d xz and yz orbitals. On the other hand, the orbital-weight variation on the electron pockets involves both the 3d xz/yz and xy orbitals. We can therefore expect that orbital selectivity will be most clearly seen in the variation of the SC gap on the electron pockets.

Despite the isotropic SC gap observed in a number of iron-based superconductors [17–21], recent experiments have also identified an anisotropic gap along the Fermi pockets in several iron pnictides [22–25]. In particular, high-resolution ARPES [22] has revealed an anisotropic SC gap along the electron Fermi pockets in the underdoped $Na(Fe_{1-x},Co_x)As$; it becomes isotropic when the system reaches the overdoped regime. Our discussions earlier then suggest that the underdoped $Na(Fe_{1-x},Co_x)As$ is an ideal system for the study of the influence of orbital selectivity on SC pairing in general and on neutron resonance in particular.

In this paper, we study SC pairing in a five-orbital t-J_1-J_2 model for iron pnictides. We show that the orbital-selective effects of electron correlations generally give rise to orbital-selective SC gaps. In particular, we emphasize two gaps that are associated with the xz/yz and xy orbitals, respectively, which have the same A_{1g} symmetry but different pairing amplitudes. We show how this orbital-selective pairing naturally leads to a gap anisotropy and double spin resonance excitations, defined as having two peaks in the frequency dependence of the dynamical spin susceptibility at a given wave vector. Finally, we discuss the implication of the results for the ARPES and neutron scattering spectra of several SC iron pnictides.

II. MODEL AND METHOD

We consider a five-orbital t-J_1-J_2 model, which is obtained via a strong-coupling perturbative w expansion about the Mott transition (for a recent review, see Ref. [26]). The Hamiltonian

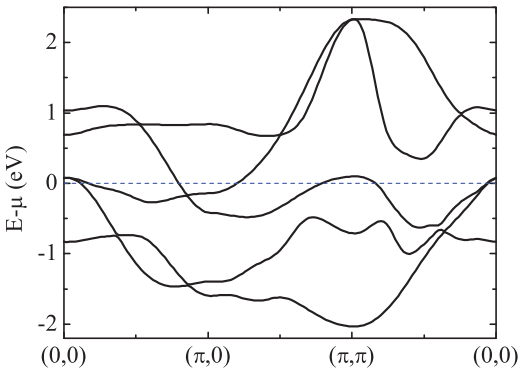

FIG. 1. (Color online) Band structure of the five-orbital tight-binding model along high-symmetry directions of the one-Fe Brillouin zone. The chemical potential is chosen such that the electron filling is at $n = 6.02$.

[27–29] reads

$$H = -\sum_{i<j,\alpha,\beta,s}\left(t_{ij}^{\alpha\beta}c_{i\alpha s}^{\dagger}c_{j\beta s} + \text{H.c.}\right) + \sum_{i,\alpha}(\epsilon_{\alpha}-\mu)n_{i\alpha} + \sum_{\langle ij\rangle,\alpha,\beta} J_1^{\alpha\beta}\left(\mathbf{S}_{i\alpha}\cdot\mathbf{S}_{j\beta} - \frac{1}{4}n_{i\alpha}n_{j\beta}\right) + \sum_{\langle\langle ij\rangle\rangle,\alpha,\beta} J_2^{\alpha\beta}\left(\mathbf{S}_{i\alpha}\cdot\mathbf{S}_{j\beta} - \frac{1}{4}n_{i\alpha}n_{j\beta}\right), \quad (1)$$

with the constraint of prohibiting double occupancy of the holes for each orbital. Here, $c_{i\alpha s}^{\dagger}$ creates an electron at site i, in orbital α and spin projection s; μ is the chemical potential to fix the total electron number n. The orbital index $\alpha = 1,2,3,4,5$ corresponds, respectively, to the five Fe $3d$ orbitals xz, yz, x^2-y^2, xy, and $3z^2$-r^2. The parameters $t_{ij}^{\alpha\beta}$ refer to the tight-binding hopping matrix, and ϵ_{α} denotes the onsite potential that reflects the crystal level splitting. For definiteness, we consider the case of NaFeAs, and we obtain the tight-binding parameters by fitting its local-density approximation (LDA) band structure. The details of the parametrization are discussed in Appendix A. The band structure of the five-orbital tight-binding model is shown in Fig. 1. The nearest-neighbor (n.n., $\langle ij\rangle$) and next-nearest-neighbor (n.n.n., $\langle\langle ij\rangle\rangle$) exchange couplings are denoted by $J_1^{\alpha\beta}$ and $J_2^{\alpha\beta}$, respectively. The spin operator is $\mathbf{S}_{i\alpha} = \frac{1}{2}\sum_{s,s'} c_{i\alpha s}^{\dagger}\boldsymbol{\sigma}_{ss'}c_{i\alpha s'}$ and the density operator $n_{i\alpha} = \sum_s c_{i\alpha s}^{\dagger}c_{i\alpha s}$, where $\boldsymbol{\sigma}$ represents the Pauli matrices. The double-occupancy prohibiting constraint from the fermion is implicitly incorporated by the renormalization of the band structure [29,30], as was explained in some detail in the supplementary methods of Ref. [30].

In addition to the J_1 and J_2 exchange interactions, a biquadratic interaction also arises from a perturbative w expansion. This term is important in understanding the anisotropic spin excitations in the parent pnictides [31,32]. However, for superconductivity, it only provides higher-order corrections to the pairing amplitudes. Hence, in this paper we will focus on the SC pairing in the above t-J_1-J_2 model by decomposing the exchange interactions in the spin-singlet pairing channels. In principle, the exchange couplings $J_{1(2)}^{\alpha\beta}$ will be a matrix in orbital space [27,33,34]. However, for the purpose of studying possible new characteristics of the spin resonance in the regime where the SC gap is anisotropic through an orbital-selective pairing, we simplify the problem by taking $J_{1(2)}^{\alpha\beta} = J_{1(2)}\delta_{\alpha\beta}$ (and take J_2 to be the energy unit). Correspondingly, we consider intraorbital pairing. For this model, there are then 20 different pairing channels, each with an amplitude and a phase, which are self-consistently determined.

We also calculate the dynamical spin susceptibility in the SC state. At wave vector $\mathbf{q}$ and Matsubara frequency ω_n, the spin susceptibility

$$\chi(\mathbf{q},i\omega_n) = \sum_{\alpha\beta}\chi_{\alpha,\beta}(\mathbf{q},i\omega_n), \quad (2)$$

where

$$\chi_{\alpha,\beta}(\mathbf{q},i\omega_n) = \sum_{\gamma}[\mathbf{I} + J(\mathbf{q})\boldsymbol{\chi}^0(\mathbf{q},i\omega_n)]^{-1}_{\alpha\gamma}\chi^0_{\gamma,\beta}(\mathbf{q},i\omega_n) \quad (3)$$

and

$$\chi^0_{\alpha,\beta}(\mathbf{q},i\omega_n) = \int_0^{1/T} d\tau\, e^{i\omega_n\tau}\langle\mathcal{T}_{\tau}[S^-_{\mathbf{q}\alpha}(\tau)S^+_{-\mathbf{q}\beta}(0)]\rangle. \quad (4)$$

Here

$$J(\mathbf{q}) = \frac{J_1}{2}(\cos q_x + \cos q_y) + J_2\cos q_x\cos q_y, \quad (5)$$

$S^{\pm}_{\mathbf{q}\alpha} = \frac{1}{\sqrt{N}}\sum_i e^{i\mathbf{q}\cdot\mathbf{r}_i}S^{\pm}_{i\alpha}$, and $\langle\cdots\rangle$ refers to the expectation value with respect to the effective Hamiltonian. The susceptibility at real frequency ω is then obtained by an analytical continuation $i\omega_n \to \omega + i0^+$.

III. RESULTS

A. Multiorbital nature of the Fermi surface and orbital-selective pairing

The band structure and the corresponding Fermi surface in the 1-Fe BZ for the tight-binding model at electron doping $x = 0.02$ ($x = n - 6$) are shown, respectively, in Figs. 1 and 2(a). The Fermi surface contains multiple sheets with different orbital characters. The two hole pockets near (0,0) are dominated by the degenerate xz/yz orbitals; the hole pocket near (π,π) has almost completely xy orbital character. The electron pocket near $(\pi,0)$ [or $(0,\pi)$] displays a hybridized xy and yz (xz) orbital character [Fig. 2(b)]. The pairing amplitudes are also orbital-dependent. For $J_1/J_2 \lesssim 1$, the dominant pairing channel is $s_{x^2y^2}A_{1g}$ [Fig. 2(c)]. The amplitude of this pairing channel in the xy orbital is larger than that in the xz/yz orbital. The double degeneracy of the xz and yz orbitals gives rise to a subdominant $d_{x^2\text{-}y^2}$ pairing channel with the same A_{1g} symmetry. Its amplitude increases with J_1/J_2. The existence of orbital-selective multiple energy scales in pairing is a consequence of the orbital-selective electron correlation effects in the multiorbital model, with the xy orbital typically exhibiting strong correlation effects [4–6]. Correspondingly, the xy orbital has a sizable ratio of J to the renormalized bandwidth, which in turn yields a sizable pairing amplitude [30]. For $J_1/J_2 \gtrsim 1$, the dominant pairing changes to $d_{x^2\text{-}y^2}B_{1g}$, but a similar behavior of the orbital-selective pairing is also found. In the following, we limit our discussion to

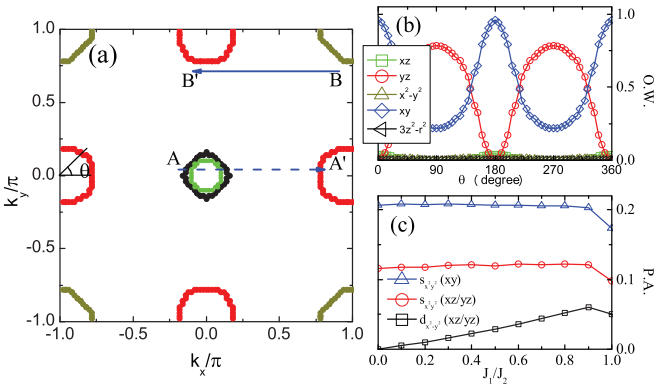

FIG. 2. (Color online) (a) Fermi surface in the one-Fe Brillouin zone of the five-orbital tight-binding model at electron doping $x = 0.02$. Angle θ parametrizes the Fermi surface pockets in momentum space. The arrows indicate the dominant scattering processes contributing to the spin resonance peaks shown in Fig. 4(a). (b) The orbital characters along the electron pocket near $(\pi,0)$. Here O.W. denotes orbital weight. (c) Evolution of the leading pairing channels in the t-J_1-J_2 model with J_1/J_2. They all have A_{1g} symmetry. Here P.A. denotes pairing amplitude.

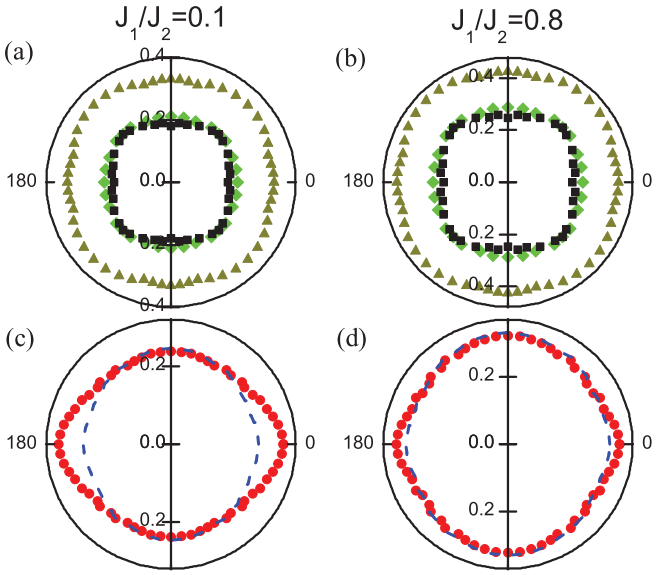

FIG. 3. (Color online) Angular dependence of the excitation gaps of BCS quasiparticles along the Fermi pockets in the t-J_1-J_2 model at $J_1/J_2 = 0.1$ [in (a) and (c)] and $J_1/J_2 = 0.8$ [in (b) and (d)], respectively. In (a) and (b), green diamonds and black squares refer to the gaps along the inner and outer hole pockets near (0,0); brown triangles refer to the gap along the hole pockets near (π,π). In (c) and (d), red circles refer to the gap along the electron pocket near $(\pi,0)$. The blue dashed line is a fit to the single parameter gap function $\Delta_0 \cos k_x \cos k_y$. The deviation from this fit implies a multigap structure of the multiorbital model (see the text).

$J_1/J_2 < 1$, where the dominant pairing $s_{x^2y^2}$ A_{1g} is consistent with the nodeless sign changing pairing observed in experiments.

B. Anisotropic superconducting gap

We now turn to how the orbital-selective pairing amplitudes and the orbital character of the Fermi surface affect the momentum distribution of the SC gaps by inducing gap anisotropy, and how the gap amplitudes and the corresponding anisotropy can be tuned by the degree of magnetic frustration of the system. We discuss and compare the results in the five-orbital t-J_1-J_2 model by taking $J_1/J_2 = 0.1$ and 0.8 for illustrative purpose. For $J_1/J_2 = 0.1$, the SC gaps are dominated by the $s_{x^2y^2}$ A_{1g} pairing channel. The amplitudes of this pairing channel in the xy and xz/yz orbitals are significantly different, resulting in two characteristic gaps $\Delta_{xy} \neq \Delta_{xz/yz}$. The excitation gap of the quasiparticles along each hole pocket is only associated with one of them [see Appendix B, Figs. 5(a) and 5(b)], and is isotropic [Fig. 3(a)] since the dominant orbital character of a hole pocket is uniform in momentum space: xy for the pocket near (π,π) and xz/yz for the pocket near (0,0). On the other hand, the gaps along the electron pockets are strongly anisotropic [Fig. 3(c)]. This is because the electron pocket has a hybridized xy and xz/yz orbital character, and the size of the gap at a particular wave vector depends on the dominant orbital character at that point. The gap anisotropy reflects these two characteristic SC gaps $\Delta_{xy} \neq \Delta_{xz/yz}$: as shown in Fig. 3(c), the gap cannot be fitted by a single gap function $\Delta_0 \cos k_x \cos k_y$, although the dominant pairing channel is $s_{x^2y^2}$ A_{1g}. Interestingly, the gap anisotropy reduces with increasing J_1/J_2, and an essentially isotropic gap along the electron pocket is recovered at $J_1/J_2 = 0.8$ [Fig. 3(d)]. To understand this, note that the pairing amplitude of the subdominant $d_{x^2-y^2}$ A_{1g} channel in the xz/yz orbital increases with J_1/J_2. With the contribution from this subdominant channel, the overall gap in the xz/yz orbital $\Delta_{xz/yz} \approx \Delta_{xy}$. This then leads to an essentially isotropic gap along the electron pockets.

C. Spin resonance excitation

The spin excitations in the SC state are also affected by the orbital-selective pairing. We have calculated the dynamical spin susceptibility in the SC state for the $J_1/J_2 = 0.1$ and 0.8 cases discussed above. The imaginary part of the susceptibility $\chi''(\mathbf{q},\omega)$ at the antiferromagnetic wave vector $\mathbf{q} = (\pi,0)$ exhibits two resonance peaks in the frequency dependence for $J_1/J_2 = 0.1$ [Fig. 4(a)]. Our detailed analysis finds that the double-peak structure of $\chi''(\mathbf{q},\omega)$ arises from the different scattering processes that connect two regimes near the electron and hole pockets, as indicated by the arrows in Fig. 2(a). By appearing in the coherence factor of the expression of $\chi''(\mathbf{q},\omega)$, the different orbital characters of the quasiparticle dispersion put a strong constraint on the scattering processes such that the spin response is enhanced only in certain regimes of the BZ, where the orbital characters of the associated hole and electron bands are compatible. For example, the dominant contribution to the lower-frequency resonance peak at ω_L [see Fig. 4(c)] is from scattering between the yz orbital in regime A and the xy orbital in regime A', as indicated by the dashed arrow in Fig. 2(a). The higher-frequency resonance peak at ω_H, on the other hand, is mainly associated with scattering within the xy orbital between regimes B and B' [see Figs. 4(c) and 2(a)]. As a rough estimate, the resonance frequency $\omega \lesssim E_h + E_e$, where E_h and E_e are, respectively, the excitation gaps of

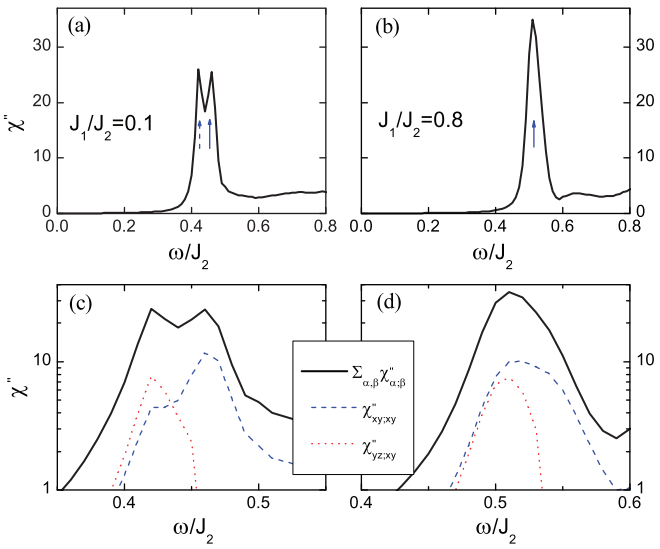

FIG. 4. (Color online) Calculated imaginary part of the dynamical spin susceptibility $\chi''(\mathbf{q},\omega)$ at wave vector $\mathbf{q}=(\pi,0)$ in the t-J_1-J_2 model for $J_1/J_2=0.1$ [in (a) and (c)] and $J_1/J_2=0.8$ [in (b) and (d)], respectively. Also shown in (c) and (d): the orbital-resolved dominant components of the susceptibility.

the corresponding hole- and electron-like quasiparticles, i.e., $h=A,B$ and $e=A',B'$. Given the similar orbital character and the proximity to the equivalent points along the Fermi surface, $E_{A'}\approx E_{B'}$. But the different orbital characters make $E_A\neq E_B$ for $J_1/J_2=0.1$. (See Appendix B for more details.)

Therefore, $\omega_L\neq\omega_H$; when this difference is sufficiently large, two resonances appear in the frequency-dependent spectrum. As J_1/J_2 increases, both E_A and E_B increase. But due to the subdominant $d_{x^2\text{-}y^2}$ channel in the xz/yz orbital, E_A increases faster, and $E_A\approx E_B$ for $J_1/J_2=0.8$. We thus obtain a single resonance peak at $\omega_L\approx\omega_H$, as shown in Figs. 4(b) and 4(d); the multiorbital effect is then reflected in the broadening of the peak.

IV. DISCUSSIONS

Our results elucidate how the orbital selectivity of electron correlations influences superconductivity. We show that the orbital-selective pairing gives rise to gap anisotropy along a Fermi surface with hybridized orbital characters. The magnetic frustration may compete with the orbital selectivity and tune the gap anisotropy. Although we used $J_1/J_2=0.1$ to illustrate the simultaneous existence of gap anisotropy and double resonance, this effect persists to $J_1/J_2\approx 0.5$. This parameter regime is relevant to experiments: we have estimated via a J_1-J_2-K model that $0.5\lesssim J_1/J_2\lesssim 1.5$ for $BaFe_2As_2$ [32] and $0.4\lesssim J_1/J_2\lesssim 1.2$ for NaFeAs [35]. The range may be further widened with the interorbital exchange couplings. Our results are particularly pertinent to the anisotropic SC gap along the electron pockets in the underdoped $Na(Fe_{1-x},Co_x)As$ observed in recent ARPES measurements [22]. We are also able to understand the evolution from the anisotropic to the isotropic gap with increasing electron doping: Since the orbital selectivity decreases with electron doping concentration, we expect that the gap will become less anisotropic in the overdoped regime [36].

In previous theoretical works, the anisotropic SC gaps are discussed within the Fermi surface nesting picture [37,38]. Particularly in the underdoped regime, the coexistence of antiferromagnetism and superconductivity may also lead to an anisotropic gap along the reconstructed Fermi surface [39]. In this scenario, the Fermi surface is reconstructed for both the electron and hole pockets. But experimentally, the gap anisotropy was only observed along electron pockets, and the Fermi surface reconstruction for the gap anisotropy was not observed [22]. It is therefore unlikely that the observed anisotropic gap is primarily driven by the coexistence of superconductivity with antiferromagnetic order.

The anisotropic gap along the electron pocket has also been observed in LiFeAs via ARPES [23], and in hole-doped $BaFe_2As_2$ via Raman scattering [25]. Given the very different Fermi surface geometry but similar orbital weights along the electron pocket in these materials, it is likely that the gap anisotropy is associated with orbital selectivity. Particularly for hole-doped $BaFe_2As_2$, because hole doping tends to increase the orbital selectivity of electron correlations [40], it is natural to propose that the mechanism advanced here underlies this experimental observation as well.

We have also shown that the frequency dependence of the dynamical spin susceptibility at $(\pi,0)$ displays a resonance whose width is enhanced by the orbital-selective SC gap. When the degree of orbital selectivity is sufficiently strong, the resonance peak may be split into two. Recently, experimental evidence for this has come from neutron-scattering observation of double spin resonances in the electron underdoped NaFeAs system [41]. We stress that the double-resonance feature we have discussed refers to two peaks in the frequency dependence of the dynamical spin susceptibility at one single wave vector. This is very different from weak-coupling calculations. For instance, the calculations of Ref. [42] show only one peak in the frequency dependence at any given wave vector, either at the commensurate $\mathbf{q}=(\pi,0)$ or at an incommensurate $\mathbf{q}$. In our case, the peaks in the frequency dependence appear at the same commensurate wave vector $\mathbf{q}=(\pi,0)$; this wave vector is determined by the $\mathbf{q}$ dependence of $J(\mathbf{q})$. As the wave vector moves away from $\mathbf{q}=(\pi,0)$, the two resonances disperse individually; there are still two peaks in the frequency dependence.

Furthermore, we have become aware of another recent theoretical work [43] which considered the effect of twinning on the spin neutron resonances. In that work, the two resonances at the same wave vector $(\pi,0)$ come from two twinned domains, and in each domain there is still a single resonance at each wave vector.

Finally, the degree of electron correlations remains a central issue in the iron-based superconductors [27,33,44–56]. This issue is typically probed in the normal state, through the bad-metal phenomenology in the optical spectrum [57] or the orbital selectivity in the ARPES spectrum [10,11]. Our theoretical results here suggest that this issue can also be fairly directly probed through the orbital selectivity of the gap function in the SC state. ARPES studies along this direction are already quite realistic [58,59], and we anticipate that a

considerable amount of new insights will be derived through further studies.

V. CONCLUSIONS

Our calculation on the superconducting pairing in a five-orbital t-J_1-J_2 model for iron pnictides reveals an orbital-selective gap structure due to the strong electron correlation effects. While both gaps have $s_{x^2y^2}$ A_{1g} symmetry, the different orbital character gives rise to gap anisotropy along the electron pockets. The orbital-selective pairing leads to a broadened neutron resonance at the antiferromagnetic ordering wave vector $\mathbf{q} = (\pi,0)$ in the superconducting state. This resonance may even be split into two peaks if the gap is sufficiently anisotropic. Our results have important implications for the ARPES and neutron measurements on the electron underdoped NaFeAs, as well as the Raman scattering results on the hole-doped $BaFe_2As_2$. More generally, our results point to ways of probing electron correlation effects of the iron pnictides through the single-particle and spin responses in their superconducting state.

ACKNOWLEDGMENTS

We thank P. Dai, D. H. Lu, and C. L. Zhang for useful discussions. This work was supported in part by NSF Grant No. DMR-1309531, the Robert A. Welch Foundation Grant No. C-1411 (R.Y. & Q.S.), the National Science Foundation of China Grant No. 11374361 (R.Y.), the Alexander von Humboldt Foundation (Q.S.), and the National Nuclear Security Administration of the U.S. DOE at LANL under Contract No. DE-AC52-06NA25396 and the U.S. DOE Office of Basic Energy Sciences (J.X.Z.). One of us (Q.S.) acknowledges the hospitality of the Aspen Center for Physics (NSF Grant No. 1066293), the Institute of Physics of the Chinese Academy of Sciences, and the Karlsruhe Institute of Technology.

APPENDIX A: TIGHT-BINDING PARAMETRIZATION

To obtain the tight-binding parameters, we perform local-density approximation (LDA) calculations for NaFeAs, and we fit the LDA band structure to the tight-binding Hamiltonian.

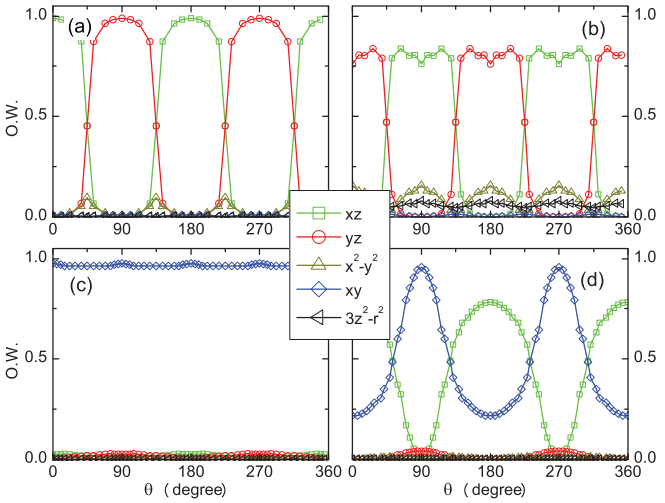

FIG. 5. (Color online) Orbital weights along the Fermi surface of the five-orbital tight-binding model at $n = 6.02$. (a) and (b) Inner and outer hole pockets near (0,0); (c) hole pockets near (π,π); (d) electron pocket near $(0,\pi)$.

We use the form of the five-orbital tight-binding Hamiltonian given in Ref. [47]. The tight-binding parameters so derived are listed in Table I.

Figure 1 shows the band structure of the five-orbital tight-binding model for electron density $n = 6.02$, corresponding to $x = 0.02$ electron doping. The corresponding Fermi surface is shown in Fig. 2(a). The Fermi surface consists of three hole pockets and two electron pockets. They have very different orbital compositions. We show the orbital weights of the hole and electron pockets in Figs. 2(b), 5, and 6(a).

APPENDIX B: MOMENTUM DISTRIBUTION OF THE EXCITATION GAP OF THE QUASIPARTICLES

In the conventional BCS theory for a single-band model with s-wave pairing symmetry, the superconducting gap Δ is momentum-independent, and the excitation gap for the BCS quasiparticles is $E(\mathbf{k}) = \sqrt{(\xi_{\mathbf{k}} - \mu)^2 + \Delta^2}$, where $\xi_{\mathbf{k}}$ and μ are, respectively, the dispersion and chemical potential of

TABLE I. Tight-binding parameters of the five-orbital model for NaFeAs.

	$\alpha=1$	$\alpha=2$	$\alpha=3$	$\alpha=4$	$\alpha=5$		
ϵ_α	−0.10818	−0.10818	−0.40863	0.14158	−0.40471		
$t_\mu^{\alpha\alpha}$	$\mu=x$	$\mu=y$	$\mu=xy$	$\mu=xx$	$\mu=xxy$	$\mu=xyy$	$\mu=xxyy$
$\alpha=1$	0.01398	−0.42534	0.24665	−0.02238	−0.00638	−0.06954	0.07281
$\alpha=3$	0.34046		−0.08566	0.01052			
$\alpha=4$	0.16907		0.12337	0.00955	−0.02595		−0.03576
$\alpha=5$	−0.04400			−0.04958	0.01441		−0.05132
$t_\mu^{\alpha\beta}$	$\mu=x$	$\mu=xy$	$\mu=xxy$	$\mu=xxyy$			
$\alpha\beta=12$		0.22625	−0.06712	0.05439			
$\alpha\beta=13$	−0.32770	0.04340	0.03380				
$\alpha\beta=14$	0.00011	−0.10269	0.00780				
$\alpha\beta=15$	−0.04573	−0.14882		−0.00124			
$\alpha\beta=34$			−0.04511				
$\alpha\beta=35$	−0.25003		0.01931				
$\alpha\beta=45$		−0.13024		0.01023			

[45] K. Kuroki *et al*., Phys. Rev. Lett. **101**, 087004 (2008).
[46] I. I. Mazin *et al*., Phys. Rev. Lett. **101**, 057003 (2008).
[47] S. Graser *et al*., New J. Phys. **11**, 025016 (2009).
[48] T. Yildirim, Phys. Rev. Lett. **101**, 057010 (2008).
[49] F. Ma, Z.-Y. Lu, and T. Xiang, Phys. Rev. B **78**, 224517 (2008).
[50] C. Fang *et al*., Phys. Rev. B **77**, 224509 (2008).
[51] J. Dai *et al*., Proc. Natl. Acad. Sci. (USA) **106**, 4118 (2009).
[52] F. Yang, F. Wang, and D.-H. Lee, Phys. Rev. B **88**, 100504 (2013).
[53] Y. Zhang *et al*., Nat. Mater. **10**, 273 (2011).
[54] T. Qian *et al*., Phys. Rev. Lett. **106**, 187001 (2011).
[55] D. Mou *et al*., Phys. Rev. Lett. **106**, 107001 (2011).
[56] D. Liu *et al*., Nat. Commun. **3**, 931 (2012).
[57] M. M. Qazilbash *et al*., Nat. Phys. **5**, 647 (2009).
[58] T. Shimojima *et al*., Science **332**, 564 (2011).
[59] W. Malaeb *et al*., Phys. Rev. B **86**, 165117 (2012).